In vitro evaluation of nanoerythrosomes cytotoxicity and uptake in pancreatic endothelial cells: implications for β-cells imaging applications

Vitale Miceli,[1,$] Marco Fornasier,[2,3,$] Matteo Bulati,[1] Giandomenico Amico,[1,4] Pier Giulio Conaldi,[1] Anna Casu,[5,6] and Sergio Murgia[3,7,]**

[1] Research Department, IRCCS ISMETT (Istituto Mediterraneo per i Trapianti e Terapie ad Alta Specializzazione), Palermo, Italy

[2] Department of Chemical and Geological Sciences, University of Cagliari, s.s. bivio Sestu, 09042-I Monserrato, Italy

[3] CSGI, Consorzio Interuniversitario per lo Sviluppo dei Sistemi a Grande Interfase, via della Lastruccia 3, 50019 Sesto Fiorentino, Florence, Italy

[4] Ri.MED Foundation, Via Bandiera 11 – I-90133 Palermo, Italy

[5] Translational Research Institute– AdventHealth, Orlando, Florida 32804, USA

[6] Department of Diagnostic and Therapeutic Services, IRCCS ISMETT (Istituto Mediterraneo per i Trapianti e Terapie ad alta specializzazione), via E. Tricomi 5, I-90127 Palermo, Italy

[7] Department of Life and Environmental Sciences, University of Cagliari and CSGI, via Ospedale 72, I-09124 Cagliari, Italy

[$] These authors equally contributed to this work.

*Corresponding authors: Sergio Murgia, murgias@unica.it; Anna Casu, Anna.Casu@AdventHealth.com

Keywords: red blood cells, nanoerythrosomes, vesicles, bio-inspired materials, diabetes, cross-linking

Abstract

Biomolecule targeted imaging represents one of the most difficult challenges in medicine. Nanoerythrosomes (NERs) are nano-vesicles obtained after lysis of red blood cells, and they are promising tools for drug delivery and imaging. In this work, a formulation based on NERs functionalized with 7-amino-3-methylcoumarin *via* cross-linking was tested on rat INS-1E and mouse MIN6 β-cells and endothelial MSI cell lines. First, morphology, size, ζ-potentials, and spectroscopic properties of the aggregates were investigated, highlighting that the functionalization did not significantly affect the nanoparticles' physicochemical features. *In vitro*, the nanoparticles did not significantly affect the proliferation and function of INS-1E and MIN6 β-cells at different concentrations. Only at the highest concentration tested on the MSI cell line, the formulation inhibited proliferation. Furthermore, NERs aggregates were not internalized in both INS-1E and MIN6 cell lines, while a diffuse fluorescence was noticed in the cytosol of the MSI cell line at the highest concentrations. These findings proved that NERs formulations might represent a new nano-tool for β-cells imaging as a part of a strategy aimed to prevent any intracellular accumulation, thus reducing/avoiding side effects.

INTRODUCTION

Diabetes is a metabolic disease whose principal feature is the reduced functionality of pancreatic β-cells both in type 1 diabetes (T1D), where pancreatic β-cells are damaged by the immune system [1], and in type 2 diabetes, where clinically evident hyperglycemia manifests only when the β-cell function is reduced.[2] Therefore, there is a clinical need for early detection and monitoring of the β-cells mass during disease progression and monitoring β-cells replacement therapies[3, 4] or prevention treatments.[5] Despite several attempts, there are no standardized and clinically applicable methods for imaging of β-cells mass.[6] The ideal labeling agent should be able to reach the β-cells, be non-toxic, retained by target cells for an appropriate time at high concentration and, after fulfilling the purpose, it should present a fast clearance *in vivo*. - Nanoparticle (NP) agents might have these characteristics and be used to carry drugs or as imaging agents on the tissue of interest.

Several NPs have been studied and designed for cell tracking and theranostic purposes.[7-9] Hard and soft matter-based carriers such as silica NPs[10-12], lamellar[13-15], and non-lamellar[16-24] lipid liquid crystalline nanoparticles have been shown to be good candidates in nanomedicine for in vitro and in vivo applications. Although significant progress has been made so far, practical limitations such as insufficient biocompatibility and short *in vivo* half-life have hindered their application in nanomedicine. [25] The passive nanoparticle diffusion into diseased tissue with damaged or incomplete endothelium (Enhanced Permeation and Retention effect seen in oncology) [26, 27] has been hypothesized in T1D, where islet microvasculature increased permeability favors nanoparticle extravasation. [28, 29] Conjugating specific ligands onto nanoparticle surfaces will increase cellular uptake by receptor-mediated endocytosis, providing an advantage to passive diffusion, enhancing specificity for low abundant cell targets.

Recently, advantages of cell-derived aggregates have emerged, such as long-circulation time and monitorable drug delivery. [30-32] Furthermore, their surface can be functionalized using ligands that can bind specific target cells' receptors. [33, 34]

Among these biomimetic nanomaterials, red blood cells (RBCs) have successfully produced biocompatible and non-immunogenic carriers for both medical bio-imaging and drug delivery. [30, 35-37] The so-called ghosts, obtained after removing hemoglobin in a hypotonic environment and RBC membrane re-sealing, have been reported as efficient drug vectors. [37-39] Furthermore, since their micrometric size induces a fast *in vivo* clearance [40], they can be sonicated or extruded to produce vesicle-like structures with a small size range (100 – 200 nm) to enhance their blood circulation time. Reported for the first time by Gaudreault and collaborators in 1994, nanoerythrosomes (NERs) obtained by RBCs ghosts represent a new class of biocompatible drugs and carriers of imaging probes. [38, 41-46]

Furthermore, their rich surface tunability can be exploited to bind labeling agents for optical imaging: since NERs derive from biological materials, they express on their surface several functional groups (-NH_2, -SH, -COOH) that can be used to link targeting agents, imaging probes and drugs. [44, 46] Moreover, it was recently shown how cross-linking and click chemistry could aid in decorating NERs surfaces to obtain fluorescently labeled nano-tools in the imaging field. [43]

Herein, a NERs dispersion functionalized with the Vis-emitter 7-amino-3-methylcoumarin (AMC) was tested *in vitro* to develop a biocompatible targeted tool for β-cell imaging. The nanoparticle morphology, size, and ζ-potential have been investigated, as well as the uptake and cytotoxicity against MSI cell line (mouse pancreatic islet endothelial cells), INS-1E and MIN6 cell lines (rat and mouse pancreatic β-cells respectively) representing sequential targets of the imaging tool.

EXPERIMENTAL SECTION

Chemicals and materials

During a routine clinical examination, bovine blood was withdrawn from a healthy cow (Istituto Zooprofilattico della Sardegna). To avoid red blood cells coagulation, blood samples were mixed

with 1.5 mg of Na-EDTA . Before any further manipulation, blood samples were stored at 4 ° and used within 2 hours after withdrawal.

Reagents were purchased from the following companies: 7-amino-4-methylcoumarin (AMC) and Glutaraldehyde 50 % v/v from TCI Chemicals (Belgium). Sodium phosphate monobasic, sodium phosphate dibasic, sodium chloride, and potassium chloride from Sigma Aldrich S.r.l. (Italy) and mixed to prepare a 10 mM phosphate buffered saline (PBS) at pH 7.4.

For standards preparations, a Milli-Q system (Millipore Corporation, Bedford, MA, USS) was used to purify fresh distilled water. The preparation was filtered with a 0.22 μm pore size hydrophilic Millipore filter prior to use.

Nanoparticles preparation

NERs preparation protocol

The preparation method of nanoerythrosomes has been reported in recent papers. [38, 43] At first, 100 mL of cold PBS solution at pH 7.4 was used to dilute 40 mL of whole bovine blood. This solution was then centrifuged for 15 minutes at 4 °C at 1859 g to remove plasma containing supernatant , while pelleted RBCs were washed with 30 mL of cold PBS solution at pH 7.4 before being dispersed. The process was repeated several times (usually three) to obtain a colorless and transparent supernatant . Finally, pelleted RBCs were resuspended in 30 mL of cold hypotonic solution (0.5 % wt of NaCl) and incubated in a cold bath for 30 minutesobtaining a dark red solution. This solution was then centrifuged at 10,706 g for 15 minutes at 4 °C. Finally, after removing the supernatant, the pellet was further washed and resuspended in a cold PBS solution at pH 7.4. This process was repeated (usually three times) until the pellet became light-yellow. The pellet was finally washed three times in 30 mL of cold PBS solution at pH 7.4 and centrifuged at 24,088 g for 15 minutes at 4 °C. the final preparation was resuspendedin PBS.

Finally, to form the nanoerythrosomes the light-yellow pellet resuspended in PBS at pH 7.4 was sonicated for 5 minutes with a tip-sonicator (amplitude of 90 %, 1 s ON, and 1 s OFF). The solution

was then filtered thrice through a 2.7 μm pore size membrane (Millipore). A to obtain a bluish and homogeneous colloidal dispersion of NERs after further 10 minutes of sonication (same conditions as before).

Fluorescent Labeling of NERs

Glutaraldehyde was used as a cross-linking agent to label NERs surface with fluorescence. First, 1 mL of NERs formulation at pH 7.4 was mixed with 100 μL of 0.5 % v/v solution of glutaraldehyde. Subsequently, 1 mg of AMC (a fluorescent dye) was mixed at room temperature and in the dark to the solution with gentle stirring for one hour. To stop the reaction, a solution of glycine 15 % v/v in PBS at pH 7.4 was added. Then, the formulation was stored overnight at 25 °C. The light-yellow solution obtained after this step was purified from the excess fluorophore by dialysis as follows: a dialysis tubing cellulose membrane (14 kDa molecular weight cutoff, purchased from Sigma Aldrich) was loaded with 2 mL of formulation and dialyzed against 2 L of PBS pH 7.4 for two hours by replacing PBS (at room temperature and in the dark) after one hour. This NER-AMC formulation was stored at 25 °C, ready for use.

NERs characterization

Dynamic light scattering and electrophoretic mobility measurements

Before any measurements the NER dispersions were diluted at 1:50 in 10 mM PBS pH 7.4. The apparent hydrodynamic diameter (D_H) and polydispersity index (PDI) of the formulations were recorded using a ZetaSizer Nano ZS by Malvern Instruments (Malvern, UK). The measurements were performed at a backscattering angle of 173° and using a He-Ne laser at 663 nm, while keeping the temperature at (25.0 ± 0.1) °C. [47] The same apparatus was adopted to perform electrophoretic mobility measurements to evaluate the ζ–potential for the formulation, again after dilution 1:50 in PBS pH 7.4. The reported D_H (intensity-weighted), the PDI (obtained from a second-order Cumulant analysis), and the ζ-potential are averages from at least six sequential measurements.

Cryo-TEM measurements

Samples morphology was observed using a transmission electron microscope (JEM-2200FS, JEOL). The microscope equipment included a field-emission electron source and an in-column energy filter (omega filter). Low-dose conditions were used to record the images, with 15 eV slit width in place, using an acceleration voltage of 200 kV on a bottom-mounted TemCam-F416 camera (TVIPS). Samples were prepared using an automatic plunge freezer system (Leica Em GP) with the environmental chamber operating at 90 % of relative humidity and 21.0 °C. To remove liquid in excess, a NERs or NERs-AMC formulation droplet of 4 μL was deposited on a lacey formvar carbon-coated grid (Ted Pella) and blotted with filter paper. Then, to provide the rapid vitrification of the sample in its native state, the grid was plunged into liquid ethane (around –183 °C). Using a cryo-transfer tomography holder (Fischione Model 2550, the specimens were stored in liquid nitrogen (–196 °C) before Cryo-TEM measurements.

Photophysical measurements

NER-AMC emission and absorption spectra were acquired using a Win-CaryVarian Fluorimeter and a Win-CaryVarian UV-Vis double-beam spectrophotometer, respectively. The spectra were measured in 1 cm quartz cuvettes, while the pure solvent or the mixture MeOH/PBS 3:1 were ued to subtract the background. The slits aperture for excitation and emission acquisition in fluorescence experiments were, respectively 5.0 and 2.5.

Cell culture

The mouse MSI pancreatic islet endothelial cells was purchased from the American Type Culture Collection (ATCC, Manassas, VA, USA). The rat INS-1E pancreatic β-cell line was kindly provided by Dr. A. Natalicchio (University of Bari, Italy). The mouse MIN6 pancreatic β-cell line was obtained by Dr. R. Fiume (University of Bologna, Italy). INS-1E cells were cultured in RPMI 1640 (11 mM

glucose) (Invitrogen, USA) containing 10% fetal bovine serum (FBS, Hyclone, USA), HEPES (10 mM), sodium pyruvate (1 mM), L-glutamine (2 mM), 2-mercaptoethanol (50 µM), 100 U/mL penicillin, and 100 µg/mL streptomycin (Invitrogen, USA) at 37 °C and 5% CO_2 per standard protocol. MIN6 and MSI cells, were grown in DMEM (25 mM glucose) (Invitrogen, USA) containing 15% (MIN6) or 10% (MSI) FBS (FBS, Hyclone, USA) L-glutamine (2 mM), 2-mercaptoethanol (50 µM), 100 U/mL penicillin, and 100 µg/mL streptomycin (Invitrogen, USA) at 37 °C and 5% CO_2 per standard protocol.

Evaluation of cellular uptake of NERs

NERs internalization was investigated utilizing fluorescence microscopy. INS-1E, MIN6, and MSI cells (4×10^5 wells into six-well) were grown for 1, 2, 4, and 24 hours at 37 °C (5% CO_2) with or without NERs in the dilution range from 1:50 to 1:800 to evaluate the time- and concentration dependence. After the desired time, the cells were washed with PBS, and fluorescent images were taken using EVOS^{tm} Microscope (Fisher Scientific, Paisley, Scotland, UK). Fluorescentintensities were determined with ImageJ software.

Assay of cell growth (xCELLigence)

Cell growth was measured using xCELLigence (ACEA, San Diego, CA) accordingly to the manufacturer's instructions. Briefly, after determining the background impedance, INS-1E cells ($5x10^4$ cells/well), MIN6 cells ($4x10^4$ cells/well), and MSI ($2x10^4$ cells/well) were cultured into 16-well plates and left for 30 minutes at room temperature before incubation in the Cell Analyzer at 37 °C and 5% CO_2. INS-1E, MIN6, and MSI cells were grown for 48, 24, and 6 hours respectively before incubation with or without NERs, during the log growth phase, in the dilution range from 1:50 to 1:800. At time point "0" the NPs were added to the cell flasks where they remain for the entire experiment. The impedance was measured every 15 minutes and expressed as cell index (CI), defined

as $(R_n - R_b)/15$, where R_n is the impedance and R_b is the background impedance. Each culture condition was performed in quadruplicate.

Glucose-stimulated insulin secretion (GSIS)

INS-1E and MIN6 cell lines were grown in standard conditions (see above 2.4 Cell culture) with or without NERs at different dilutions for 48 hours. After that, both cell types were cultured for an hour at a lower glucose concentration (5mM). GSIS was then analyzed. First, the cells were pre-incubated for 30 minutes at 37 °C in glucose-free buffer containing 0.1% BSA and NaCl (125 mM), KCl (5.9 mM), $MgCl_2$ (1.2 mM), $CaCl_2$ (1.3 mM), 25 mM HEPES pH 7.4. Then, the glucose-free buffer was replaced with the same buffer containing either 4/15 mM (INS-1E) glucoseor 2.8/25 mM (MIN6) glucose, and the cells were incubated for 1 hour at 37 °C. Supernatants were collected at the end of the incubation periods with low or high glucose concentrations and stored at -20 °C for insulin measure. Insulin was measured with an ultrasensitive enzyme-linked immunoassay (Mercodia AB, Uppsala, Sweden). After culture, the cells were counted with the Countess II (Thermo Scientific, USA).

Statistics

Data are reported as means ± standard deviations (SD). ANOVA was used to compare group differences (GraphPad Prism 6.0, La Jolla, USA). When ANOVA revealed $p < 0.05$, the data were further analyzed by Dunnet's t-tests. Differences were considered statistically significant at $p < 0.05$.

RESULTS AND DISCUSSION

NERs preparation and characterization

Nanoerythrosomes are vesicles derived from RBCs and can be prepared using different methods, typically involving sonication or extrusion processes. [32, 38] Recently, we designed a protocol derived from that published by Raghavan et collaborators[38], which allows the formulation of small and monodispersed NERs. During the RBC purification from blood samples, several centrifugations and washing steps are necessary to remove serum, pellets, and white cells from red blood cells. Incubation in a hypotonic solution releases the hemoglobin content, which is the main inner component of this kind of cell. During this step, the initially bright red pellets (RBCs precipitate during the centrifugation) decolorate due to the release of hemoglobin. The RBCs membranes are then re-sealed after another step of centrifugation in an isotonic environment. First, their micrometric size is reduced to the nanoscale using a tip sonicator. Then, an extrusion step through a 2.8 μm pore size filter is required to remove larger aggregates. Finally, the colloidal dispersion is sonicated again to yield a bluish and homogeneous solution.

Nanoerythrosomes are biological vesicles exhibiting on their surface -NH_2 terminal groups belonging to proteins, lipids, and glycoproteins.[32, 46] These functional groups can be exploited to functionalize the surface of the NPs with fluorescent probes, targeting agents, or drugs. Among several functionalization routes, the one based on cross-linking via glutaraldehyde was proved to be a successful and straightforward approach to decorating NERs surface.[43, 46] Here, the NERs dispersion was treated to bind on the surface a fluorophore, 7-ammino-3methylcoumarin (AMC), suitable for *in vitro* optical imaging investigations. The one-pot reaction took place in mild conditions (room temperature, physiological pH), and the non-reacted materials were removed from the dispersions *via* dialysis.

The morphology of the NERs and NERs-AMC samples was evaluated via cryo-TEM in an isotonic environment (10 mM PBS pH 7.4, 150 mM NaCl and 3 mM KCl). Figures 1A and B show the presence of different aggregates in the NERs sample: unilamellar vesicles (red arrows) and membranes not reassembled into vesicles (black arrows).

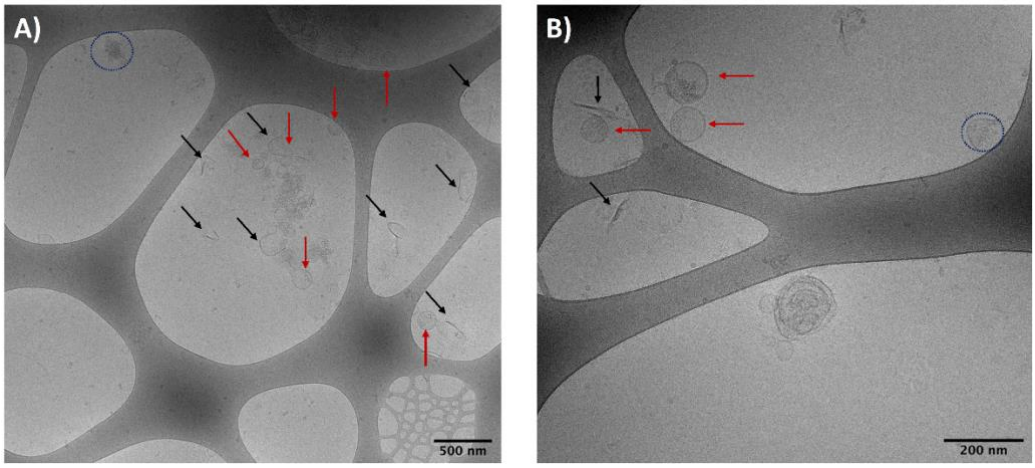

Figure 1. 10k (A) and 40k (B) magnification cryo-TEM images of the sample NERs in isotonic conditions (PBS, pH 7.4).

The high contrast aggregates (dark blue dashed circles) could be membrane proteins solubilized with their lipid surroundings by the sonication process.

After the surface functionalization with AMC via cross-linking (NERs-AMC), the samples did not show any membrane fragment, but the number of protein aggregates increased (Figure 2A, red dashed circles). Indeed, the functionalization *via* glutaraldehyde can increase the aggregation of the membrane proteins solubilized in the aqueous media after the ultrasonication step since a glutaraldehyde molecule can act as a "bridge" between two protein units. The red arrows point at unilamellar vesicles of different shapes. Concerning the latter aspect, it cannot be ruled out that the presence of glutaraldehyde at the lipid-solvent interface may affect the interfacial curvature of the system, originating non-spherical unilamellar vesicles. In Figure 2B, several nanoparticles of this kind are imaged.

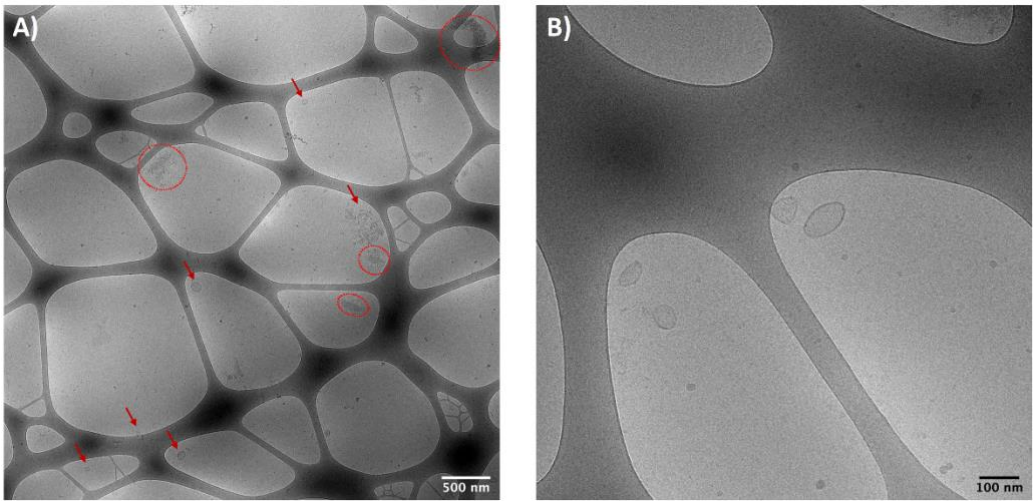

Figure 2. Cryo-TEM images of the formulation NERs-AMC at two different magnifications: x10k (A) and 40k (B).

The size and the size distribution of the two formulations were studied in terms of apparent hydrodynamic diameter and polydispersity index (PdI) by DLS (Table 1) after dilution of the formulation 1:50 in PBS to avoid interactions among nanoparticles.

Table 1. Summary of the data obtained by DLS and electrophoretic mobility measurements in 10 mM PBS pH 7.4.

Sample	**Hydrodynamic Diameter [nm]**	**Polydispersity index**	**ζ–potential [mV]**
NERs	102 ± 2	0.12 ± 0.01	- 28.3 ± 1.2
NERs-AMC	141 ± 3	0.21 ± 0.02	- 23.4 ± 2.3

These measurements evidenced that the functionalization caused a slight increase of the diameter and the PdI of the NERs dispersion. At the same time, the presence of phosphate and sodium ions only marginally alters the electrostatic potential at the nanoparticle-water interface and, therefore, the measured ζ-potential. The high negative ζ-potential exhibited by the nanoparticles guarantees adequate colloidal stability to the dispersion. Indeed, up to 5 months of storage stability was already

proven in PBS buffer.[43] Therefore, the recorded decrease of ζ-potential after the functionalization should be related to charged groups removal at the NERs-solvent interface.

The normalized absorption and emission spectra for the NERs-AMC formulation (100-fold diluted in 10 mM PBS, pH 7.4) are reported in Figure 3.

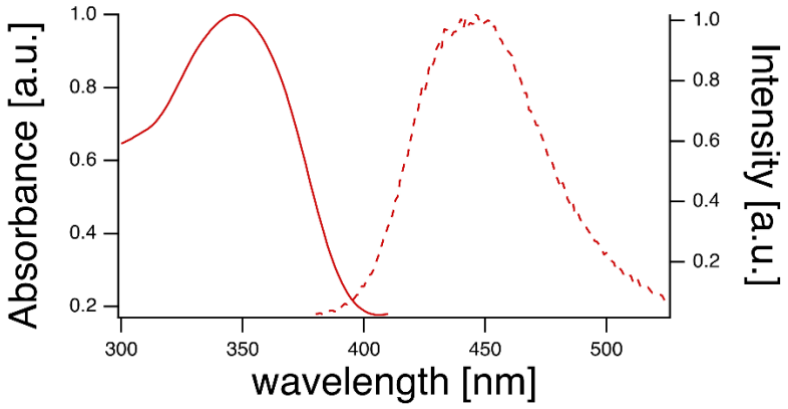

Figure 3. Normalized absorption and emission spectra of the formulation NERs-AMC in 10 mM PBS, pH 7.4 after 1:100 dilution to avoid scattering from the particles in solution.

Removal of hemoglobin is a crucial step for the preparation of NERs. It exhibits a strong absorption peak at 405 nm in PBS [48], but in Figure 3, a distinctive peak associated with the presence of hemoglobin was not observed. Consequently, it can be concluded that the residual hemoglobin content in the formulation, if any, is negligible. The preparation method of NERs could be improved by implementing a purification step, i.e., size exclusion chromatography, to remove the protein aggregates from the sample yielding a pure nanoparticles formulation. Such an approach would also underlie a possible effect of the aggregates on the physico-chemical and biological properties of the sample.

The emission wavelength of NERs-AMC, around 448 nm in 10 mM PBS at pH 7.4, represents a suitable radiation to be used for *in vitro* imaging. The fluorophore amount on NERs surface was evaluated using the calibration curve method and by reading the absorbance at 350 nm after diluting the NPs 100-fold in MeOH/PBS 3:1. The AMC concentration was $(6.3 \pm 0.4)\times10^{-5}$ M. This value perfectly agrees with that measured in our previous investigation [43] and corroborates the cross-linking reaction as a robust and reproducible way to functionalize NERs surface.

Cell internalization of NERs

NERs were incubated with INS-1E, MIN6 insulinoma cells, and endothelial cells (MSI), and the uptake was evaluated by fluorescence microscopy and quantified by digitalized images analysis. The MSI cell model maintains the characteristics of the pancreatic islet fenestrated endothelium that lack barrier characteristics [49] For this reason, it is expected that the NER will enter into the cells. INS-1 and MIN6 β-cell lines are chosen as they retain normal glucose-stimulated insulin secretion (GSIS) [50, 51]. NER behavior on these cells is not predictable. They are not expected to be internalized if not functionalized, however, their interaction with the cell surface cannot be excluded and could affect GSIS as the primary indicator of cell function. Furthermore, T1D is associated with increased microvascular permeability [28, 29] and the endothelium is damaged in islet transplantation, making NERs a suitable imaging agent for these conditions.

Therefore, the present study aims at investigating NER behavior and toxicity on cellular models crucial for NER future use for pancreatic β-cell imaging.

INS-1E and MIN6 cell lines did not internalize NERs. Moreover, the uptake was time-and concentration-independent, as varying the incubation time and the dilution within the range of dilution and application time selected for the present study did not affect the uptake. In contrast, the MSI cell line displayed green fluorescence carried by the NERs after 4 hours of exposure to 1:50 NERs (Figure 4A). In particular, Figure 4 shows that NERs were internalized only into MSI cells, and significant differences were observed among 4- and 24-hours exposure (Figure 4B).

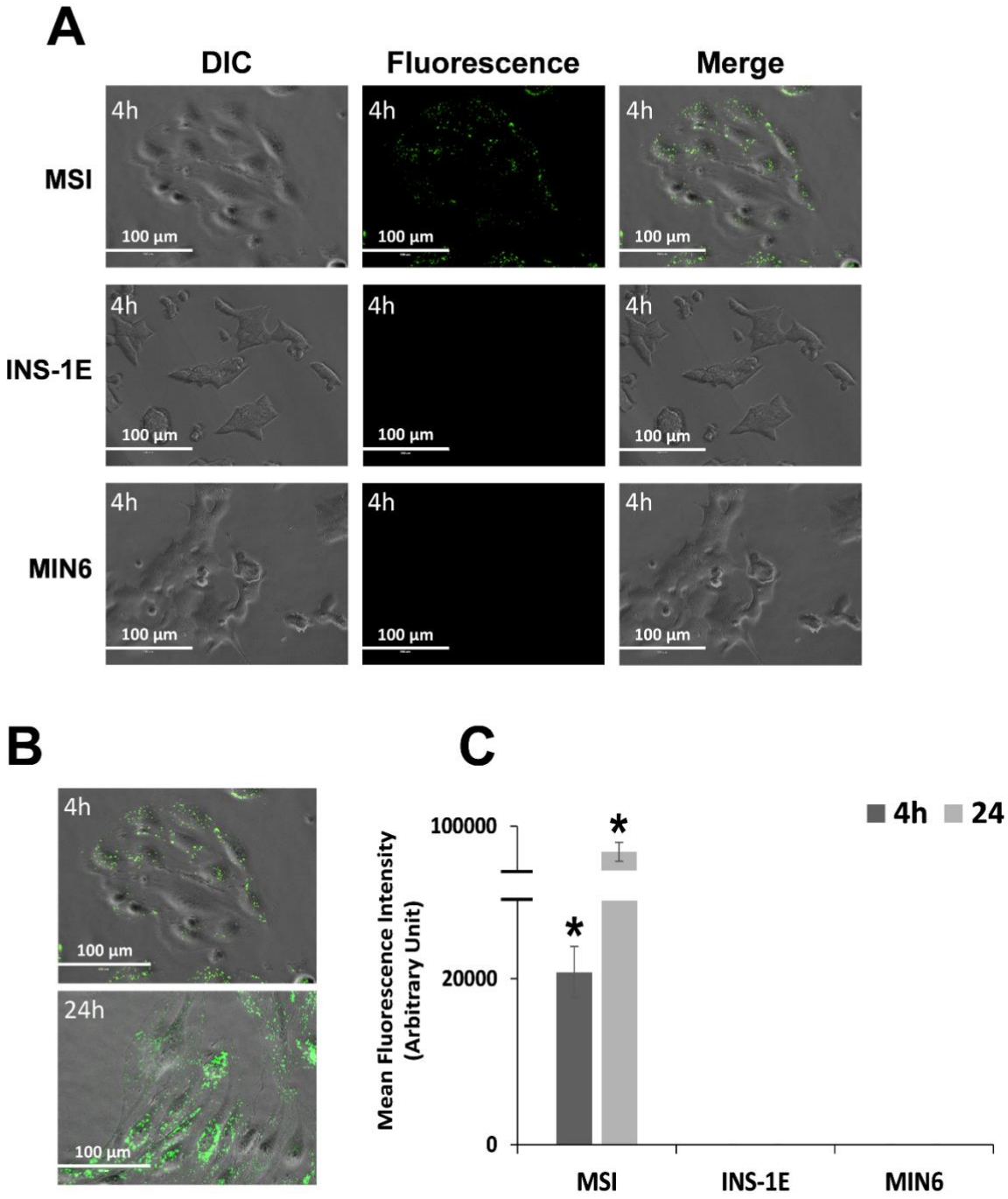

Figure 4. Microscopy analysis of NERs internalization in both pancreatic β-cell lines (INS-1E and MIN6) and endothelial cell line (MSI). (A) Representative images of INS-1E, MIN6, and MSI cells incubated with 1:50 NERs for 4 hours. (B) Representative images of MSI cells incubated with 1:50 NERs for 4 hours and 24 hours. (C) Digitized evaluation of optical fluorescence intensity after subtraction of background (using the imageJ software) of NERs internalization in INS-1E, MIN6, and MSI cells incubated with 1:50 concentration for 4 and 24 hours. Scale bar corresponds to 100 µm. DIC: differential interference contrast. All data are expressed as means ± SD of triplicates. *$p < 0.05$ *versus* control.

Furthermore, a 4.4-fold fluorescence increase was revealed in the MSI cells incubated for 24 hours compared to those treated for 4 hours (Figure 4C). Therefore, NERs have not been internalized in both INS-1E and MIN6 β-cells, whereas their uptake was time-dependent in MSI endothelial cells.

This event aligns with what has been described for other types of nanoparticles in endothelial and non-endothelial cells.[52] Further experiments are needed to understand the mechanisms of NER uptake in the MSI. However, since the cellular membrane of MSI endothelial cells expresses higher levels of caveolin [53] compared to INS-1E and MIN6 [54], it could be speculated that a caveolin mediated uptake explains nanoparticle internalization in the MSI.[52]

These results were expected. In fact, it is well known that the pancreatic islet endothelium is fenestrated, potentially favoring NERs uptake. However, this hypothesis needs to be verified with dedicated experiments in endothelial cells isolated from different body compartments.

Analysis of NERs cytotoxicity

As the NERs first contact the endothelial cells and then the pancreatic β-cells to which they are targeted, their potential toxicity to both cell types was evaluated. In particular, potential effects on cell proliferation were analyzed as a sign of cell well-being. Cell proliferation was evaluated by real-time analysis of the Xcelligence profiles.

The INS-1E and MIN6 cell proliferation profiles at all NERs concentrations did not differ from untreated cultures (Figures 5A and B, and Figures 5C and D, respectively).

Furthermore, the MSI endothelial cell proliferation exposed to NERs (from 1:100 to 1:800 dilution ratios) did not differ from untreated cells. Only the exposure to the highest NERs concentration (dilution 1:50) significantly reduced the proliferation by 18% compared to control (Figures 5E-F).

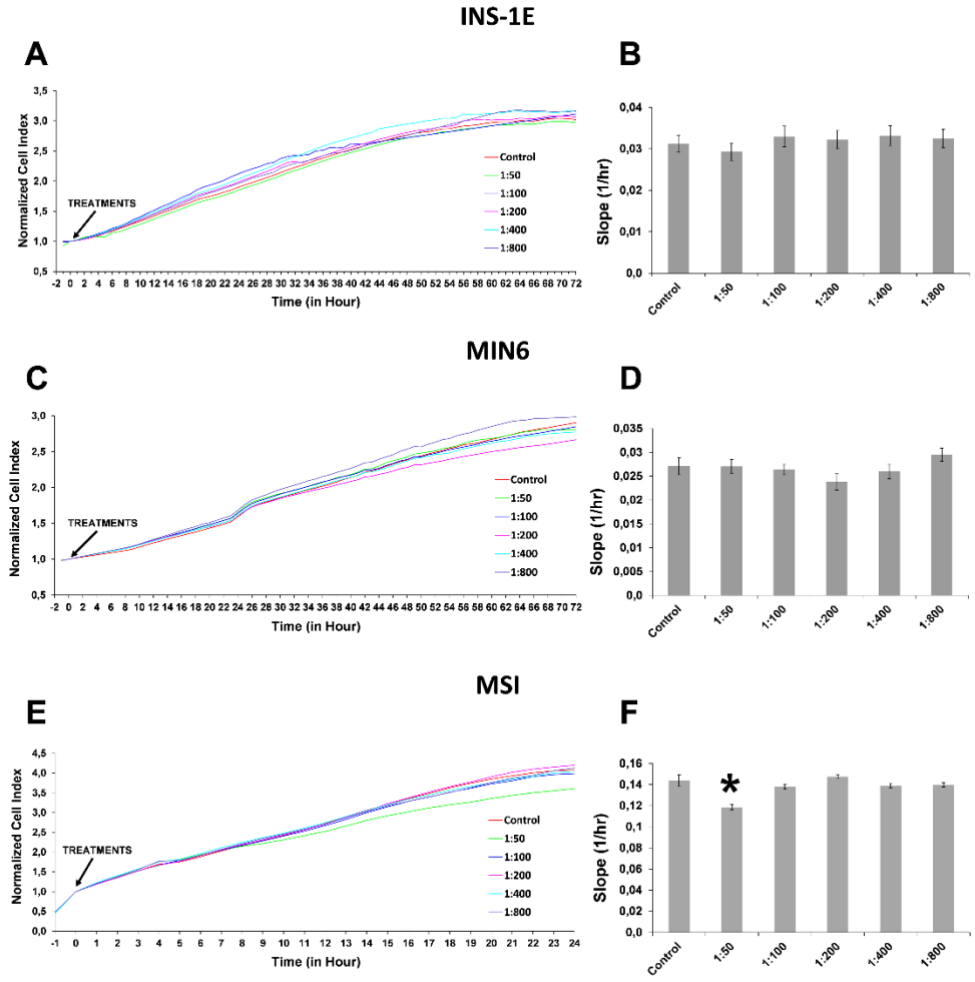

Figure 5. INS-1E, MIN6, and MSI cells growth. The cells were incubated with or without (control) NERs (from 1:50 to 1:800) to test their cytotoxicity. (A, C, and E) Real-time INS-1E, MIN6, and MSI cell growth obtained with the xCELLigence system. Cell index values were recorded every 15 min.the figures shows representative traces. (B, D, and F) Slopes of growth curves of INS-1E, MIN6, and MSI cells. Data are presented as means ± SD of n = 4. *p < 0.05 *versus* control.

Analysis of cellular function after NERs exposure

Since these NPs could be used to detect β-cells mass loss in diabetes, the insulin secretory capacity was evaluated in culture containing or not containing NERs. Glucose-stimulated insulin secretion (GSIS) was enhanced when glucose in the culture medium was increased from 4 mM to 15 mM and from 2.8 mM to 25 mM in INS-1E and MIN6 cells, respectively. No significant effect of NERs incubation at different concentrations on GSIS was seen in both cell lines (Figure 6). Thus, NERs, do not affect the proliferation and function of INS-1E and MIN6 β-cells, thus reassuring that no cell contact effect is responsible for cell function or proliferation impairment.

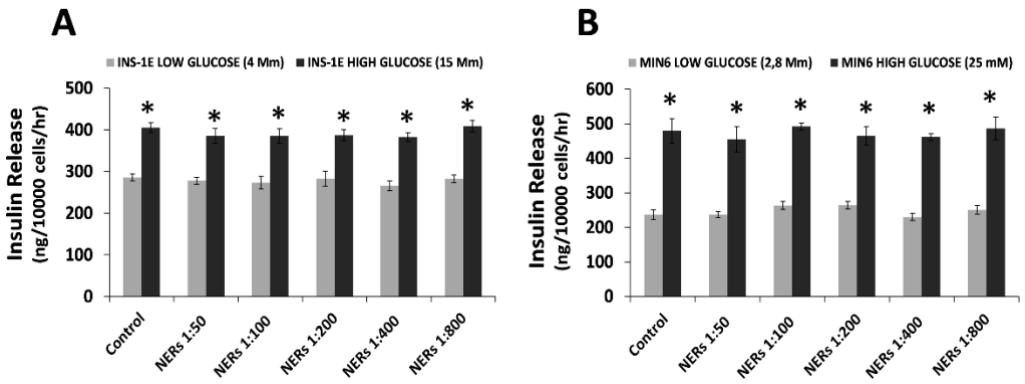

Figure 6. Glucose-stimulated insulin secretion in INS-1E and MIN6 cells. Insulin secretion after glucose stimulation (A) INS-1E and (B) MIN6 cells after 48 h incubation with or without NERs at concentrations from 1:50 to 1:800. All data are expressed as means ± SD of triplicates. *$p < 0.05$ vs. basal glucose concentration.

CONCLUSIONS

The engineering of targeted nanoparticles for imaging applications is an area of growing interest. Here we presented preliminary evidence to support the use of NERs in diabetes, where pancreatic β-cells imaging has now become a priority.

Erythrocyte-based NPs have already found applications in personal nanomedicine for cell imaging purposes. Given their nature, the immune system does not recognize them as "non-self", and they can be retained in the bloodstream for three days with a circulation half-life of nearly 40 hours.

In this scenario, NERs already applied for imaging purposes[55] and not recognized as “non-self” [56]could represent a new class of optical nano-tools for β-cells imaging, with vast implications for the understanding of diabetes pathogenesis and to monitor its preventive treatments. Labeling their surface is relatively easy (shown here and in reference[43]). The functionalization via cross-linking is robust and reproducible, and it does not significantly affect their physicochemical properties. NER formulations at different dilutions are not toxic for β-cells and are stable in the bloodstream.[57] At the highest concentration used (dilution 1:50), a modest reduction of cell proliferation was seen in the MSI cell line. Therefore, diluted NER formulations could represent a new nano-tool that might work as non-immunogenic and non-toxic platforms for optical imaging of β-cells since NERs could derive from the blood of the same subject. However, further investigations are needed to understand better

how the nanoparticle surface could be modified and if this modification might impact their biological properties to provide a new nano-tool for β-cells imaging.

A perspective could be represented by the development of a non-toxic and non-penetrable nanoparticle probe targeted with exendin-4 (a ligand for GLP-1R expressed in β-cells islets) [58] for selective targeting of pancreatic β-cells [59], and to support NER excretion after exploiting them. Furthermore, given the desired application and limited approaches to monitor the number/function of residual β-cells in T1D patients or after islet transplantation [60], not internalized modified-NERs directed towards specific cell surface targets could represent an important strategy that avoids intracellular accumulation and its potential side effects.

The ability to image pancreatic islets *via* fluorescently labeled and targeted NERs could provide a unique tool to clinicians.

Declaration of Competing Interest: The authors declare that they have no known competing financial interests or personal relationships that could have influenced the work reported in this article.

Acknowledgments

The authors kindly thank Dr. A. Natalicchio (University of Bari, Italy) and Dr. R. Fiume (University of Bologna, Italy) for providing the INS-1E and the MIN6 cells, respectively. They also thank Ms. Seema Sernovitz for the editorial review of the manuscript. Furthermore, the authors are indebted to the National Center for High-Resolution Electron Microscopy (nCHREM) at Lund University for providing access to execute the Cryo-TEM measurements and Dr. Anna M. Carnerup for her assistance and advice for these measurements. MFF Ph.D. scholarship was funded by the project POR Sardegna FSE 2014-2020. S.M. thanks Fondazione Banco di Sardegna and Regione Autonoma della Sardegna (Progetti Biennali di Ateneo Annualità 2018). The study was partially supported by IRCCS ISMETT (Istituto Mediterraneo per i Trapianti e Terapie ad Alta Specializzazione) funds.

References

1. Mathis, D.; Vence, L.; Benoist, C. beta-Cell death during progression to diabetes. *Nature* **2001,** *414*, (6865), 792-8.
2. Meier, J. J.; Bonadonna, R. C. Role of reduced beta-cell mass versus impaired beta-cell function in the pathogenesis of type 2 diabetes. *Diabetes care* **2013,** *36 Suppl 2*, S113-9.
3. Chen, C.; Cohrs, C. M.; Stertmann, J.; Bozsak, R.; Speier, S. Human beta cell mass and function in diabetes: Recent advances in knowledge and technologies to understand disease pathogenesis. *Molecular metabolism* **2017,** *6*, (9), 943-957.
4. Rickels, M. R.; Robertson, R. P. Pancreatic Islet Transplantation in Humans: Recent Progress and Future Directions. *Endocrine reviews* **2019,** *40*, (2), 631-668.
5. Umphonsathien, M.; Prutanopajai, P.; Aiam, O. R. J.; Thararoop, T.; Karin, A.; Kanjanapha, C.; Jiamjarasrangsi, W.; Khovidhunkit, W. Immediate and long-term effects of a very-low-calorie diet on diabetes remission and glycemic control in obese Thai patients with type 2 diabetes mellitus. *Food science & nutrition* **2019,** *7*, (3), 1113-1122.
6. Markmann, J. F.; Bartlett, S. T.; Johnson, P.; Korsgren, O.; Hering, B. J.; Scharp, D.; Kay, T. W.; Bromberg, J.; Odorico, J. S.; Weir, G. C.; Bridges, N.; Kandaswamy, R.; Stock, P.; Friend, P.; Gotoh, M.; Cooper, D. K.; Park, C. G.; O'Connell, P. J.; Stabler, C.; Matsumoto, S.; Ludwig, B.; Choudhary, P.; Khovatchev, B.; Rickels, M. R.; Sykes, M.; Wood, K.; Kraemer, K.; Hwa, A.; Stanley, E.; Ricordi, C.; Zimmerman, M.; Greenstein, J.; Montanya, E.; Otonkoski, T. Executive Summary of IPITA-TTS Opinion Leaders Report on the Future of beta-Cell Replacement. *Transplantation* **2016,** *100*, (7), e25-31.
7. De, K. Decapeptide Modified Doxorubicin Loaded Solid Lipid Nanoparticles as Targeted Drug Delivery System against Prostate Cancer. *Langmuir* **2021,** *37*, (45), 13194-13207.
8. Gao, Y.; Lim, J.; Teoh, S. H.; Xu, C. Emerging translational research on magnetic nanoparticles for regenerative medicine. *Chemical Society reviews* **2015,** *44*, (17), 6306-29.
9. Muthu, M. S.; Mei, L.; Feng, S. S. Nanotheranostics: advanced nanomedicine for the integration of diagnosis and therapy. *Nanomedicine* **2014,** *9*, (9), 1277-80.
10. Das, R. K.; Pramanik, A.; Majhi, M.; Mohapatra, S. Magnetic Mesoporous Silica Gated with Doped Carbon Dot for Site-Specific Drug Delivery, Fluorescence, and MR Imaging. *Langmuir* **2018,** *34*, (18), 5253-5262.
11. Iturrioz-Rodriguez, N.; Correa-Duarte, M. A.; Fanarraga, M. L. Controlled drug delivery systems for cancer based on mesoporous silica nanoparticles. *International journal of nanomedicine* **2019,** *14*, 3389-3401.
12. Lopez, V.; Villegas, M. R.; Rodriguez, V.; Villaverde, G.; Lozano, D.; Baeza, A.; Vallet-Regi, M. Janus Mesoporous Silica Nanoparticles for Dual Targeting of Tumor Cells and Mitochondria. *ACS applied materials & interfaces* **2017,** *9*, (32), 26697-26706.
13. Ciancone, M.; Bellec, N.; Cammas-Marion, S.; Dolet, A.; Vray, D.; Varray, F.; Le Goff-Gaillard, C.; Le Goff, X.; Arlot-Bonnemains, Y.; Camerel, F. Liposomes Containing Nickel-Bis(dithiolene) Complexes for Photothermal Theranostics. *Langmuir* **2019,** *35*, (47), 15121-15130.
14. Schlich, M.; Fornasier, M.; Nieddu, M.; Sinico, C.; Murgia, S.; Rescigno, A. 3-hydroxycoumarin loaded vesicles for recombinant human tyrosinase inhibition in topical applications. *Colloids and surfaces. B, Biointerfaces* **2018,** *171*, 675-681.
15. Schlich, M.; Sinico, C.; Valenti, D.; Gulati, A.; Joshi, M. D.; Meli, V.; Murgia, S.; Xanthos, T. Towards long-acting adrenaline for cardiopulmonary resuscitation: Production and characterization of a liposomal formulation. *International journal of pharmaceutics* **2019,** *557*, 105-111.
16. Barriga, H. M. G.; Holme, M. N.; Stevens, M. M. Cubosomes: The Next Generation of Smart Lipid Nanoparticles? *Angewandte Chemie* **2019,** *58*, (10), 2958-2978.
17. Bazylinska, U.; Kulbacka, J.; Schmidt, J.; Talmon, Y.; Murgia, S. Polymer-free cubosomes for simultaneous bioimaging and photodynamic action of photosensitizers in melanoma skin cancer cells. *Journal of colloid and interface science* **2018,** *522*, 163-173.

18. Biffi, S.; Andolfi, L.; Caltagirone, C.; Garrovo, C.; Falchi, A. M.; Lippolis, V.; Lorenzon, A.; Macor, P.; Meli, V.; Monduzzi, M.; Obiols-Rabasa, M.; Petrizza, L.; Prodi, L.; Rosa, A.; Schmidt, J.; Talmon, Y.; Murgia, S. Cubosomes for in vivo fluorescence lifetime imaging. *Nanotechnology* **2017,** *28*, (5), 055102.
19. Fornasier, M.; Biffi, S.; Bortot, B.; Macor, P.; Manhart, A.; Wurm, F. R.; Murgia, S. Cubosomes stabilized by a polyphosphoester-analog of Pluronic F127 with reduced cytotoxicity. *Journal of colloid and interface science* **2020,** *580*, 286-297.
20. Fornasier, M.; Pireddu, R.; Del Giudice, A.; Sinico, C.; Nylander, T.; Schillen, K.; Galantini, L.; Murgia, S. Tuning lipid structure by bile salts: Hexosomes for topical administration of catechin. *Colloids and surfaces. B, Biointerfaces* **2021,** *199*, 111564.
21. Jenni, S.; Picci, G.; Fornasier, M.; Mamusa, M.; Schmidt, J.; Talmon, Y.; Sour, A.; Heitz, V.; Murgia, S.; Caltagirone, C. Multifunctional cubic liquid crystalline nanoparticles for chemo- and photodynamic synergistic cancer therapy. *Photochemical & photobiological sciences* **2020,** *19*, (5), 674-680.
22. Miceli, V.; Meli, V.; Blanchard-Desce, M.; Bsaibess, T.; Pampalone, M.; Conaldi, P. G.; Caltagirone, C.; Obiols-Rabasa, M.; Schmidt, J.; Talmon, Y.; Casu, A.; Murgia, S. In vitro imaging of beta-cells using fluorescent cubic bicontinuous liquid crystalline nanoparticles. *Rsc Adv* **2016,** *6*, (67), 62119-62127.
23. Murgia, S.; Biffi, S.; Fornasier, M.; Lippolis, V.; Picci, G.; Caltagirone, C. Bioimaging Applications of Non-Lamellar Liquid Crystalline Nanoparticles. *Journal of nanoscience and nanotechnology* **2021,** *21*, (5), 2742-2759.
24. Naidjonoka, P.; Fornasier, M.; Palsson, D.; Rudolph, G.; Al-Rudainy, B.; Murgia, S.; Nylander, T. Bicontinuous cubic liquid crystalline phase nanoparticles stabilized by softwood hemicellulose. *Colloids and surfaces. B, Biointerfaces* **2021,** *203*, 111753.
25. Witika, B. A.; Makoni, P. A.; Matafwali, S. K.; Chabalenge, B.; Mwila, C.; Kalungia, A. C.; Nkanga, C. I.; Bapolisi, A. M.; Walker, R. B. Biocompatibility of Biomaterials for Nanoencapsulation: Current Approaches. *Nanomaterials* **2020,** *10*, (9).
26. Attia, M. F.; Anton, N.; Wallyn, J.; Omran, Z.; Vandamme, T. F. An overview of active and passive targeting strategies to improve the nanocarriers efficiency to tumour sites. *The Journal of pharmacy and pharmacology* **2019,** *71*, (8), 1185-1198.
27. Barreto, J. A.; O'Malley, W.; Kubeil, M.; Graham, B.; Stephan, H.; Spiccia, L. Nanomaterials: applications in cancer imaging and therapy. *Advanced materials* **2011,** *23*, (12), H18-40.
28. Ramirez, D. G.; Abenojar, E.; Hernandez, C.; Lorberbaum, D. S.; Papazian, L. A.; Passman, S.; Pham, V.; Exner, A. A.; Benninger, R. K. P. Contrast-enhanced ultrasound with sub-micron sized contrast agents detects insulitis in mouse models of type1 diabetes. *Nat Commun* **2020,** *11*, (1), 2238.
29. Turvey, S. E.; Swart, E.; Denis, M. C.; Mahmood, U.; Benoist, C.; Weissleder, R.; Mathis, D. Noninvasive imaging of pancreatic inflammation and its reversal in type 1 diabetes. *The Journal of clinical investigation* **2005,** *115*, (9), 2454-61.
30. Su, J.; Sun, H.; Meng, Q.; Zhang, P.; Yin, Q.; Li, Y. Enhanced Blood Suspensibility and Laser-Activated Tumor-specific Drug Release of Theranostic Mesoporous Silica Nanoparticles by Functionalizing with Erythrocyte Membranes. *Theranostics* **2017,** *7*, (3), 523-537.
31. Tan, S.; Wu, T.; Zhang, D.; Zhang, Z. Cell or cell membrane-based drug delivery systems. *Theranostics* **2015,** *5*, (8), 863-81.
32. Zhang, H. Erythrocytes in nanomedicine: an optimal blend of natural and synthetic materials. *Biomaterials science* **2016,** *4*, (7), 1024-31.
33. Luk, B. T.; Zhang, L. Cell membrane-camouflaged nanoparticles for drug delivery. *Journal of controlled release* **2015,** *220*, (Pt B), 600-7.
34. Tsai, R. K.; Rodriguez, P. L.; Discher, D. E. Self inhibition of phagocytosis: the affinity of 'marker of self' CD47 for SIRPalpha dictates potency of inhibition but only at low expression levels. *Blood cells, molecules & diseases* **2010,** *45*, (1), 67-74.

35. Rao, L.; Xu, J. H.; Cai, B.; Liu, H.; Li, M.; Jia, Y.; Xiao, L.; Guo, S. S.; Liu, W.; Zhao, X. Z. Synthetic nanoparticles camouflaged with biomimetic erythrocyte membranes for reduced reticuloendothelial system uptake. *Nanotechnology* **2016,** *27*, (8), 085106.
36. Ren, X.; Zheng, R.; Fang, X.; Wang, X.; Zhang, X.; Yang, W.; Sha, X. Red blood cell membrane camouflaged magnetic nanoclusters for imaging-guided photothermal therapy. *Biomaterials* **2016,** *92*, 13-24.
37. Wang, C.; Huang, J.; Zhang, Y.; Jia, H.; Chen, B. Construction and evaluation of red blood cells-based drug delivery system for chemo-photothermal therapy. *Colloids and surfaces. B, Biointerfaces* **2021,** *204*, 111789.
38. Kuo, Y. C.; Wu, H. C.; Hoang, D.; Bentley, W. E.; D'Souza, W. D.; Raghavan, S. R. Colloidal Properties of Nanoerythrosomes Derived from Bovine Red Blood Cells. *Langmuir* **2016,** *32*, (1), 171-9.
39. Tang, J. C.; Vankayala, R.; Mac, J. T.; Anvari, B. RBC-Derived Optical Nanoparticles Remain Stable After a Freeze-Thaw Cycle. *Langmuir* **2020,** *36*, (34), 10003-10011.
40. Valkonen, S.; van der Pol, E.; Boing, A.; Yuana, Y.; Yliperttula, M.; Nieuwland, R.; Laitinen, S.; Siljander, P. R. Biological reference materials for extracellular vesicle studies. *European journal of pharmaceutical sciences* **2017,** *98*, 4-16.
41. Deak, R.; Mihaly, J.; Szigyarto, I. C.; Beke-Somfai, T.; Turiak, L.; Drahos, L.; Wacha, A.; Bota, A.; Varga, Z. Nanoerythrosomes tailoring: Lipid induced protein scaffolding in ghost membrane derived vesicles. *Materials science & engineering. C* **2020,** *109*, 110428.
42. Desilets, J.; Lejeune, A.; Mercer, J.; Gicquaud, C. Nanoerythrosomes, a new derivative of erythrocyte ghost: IV. Fate of reinjected nanoerythrosomes. *Anticancer research* **2001,** *21*, (3B), 1741-7.
43. Fornasier, M.; Porcheddu, A.; Casu, A.; Raghavan, S. R.; Jonsson, P.; Schillen, K.; Murgia, S. Surface-modified nanoerythrosomes for potential optical imaging diagnostics. *Journal of colloid and interface science* **2021,** *582*, (Pt A), 246-253.
44. Gupta, N.; Patel, B.; Nahar, K.; Ahsan, F. Cell permeable peptide conjugated nanoerythrosomes of fasudil prolong pulmonary arterial vasodilation in PAH rats. *European journal of pharmaceutics and biopharmaceutics* **2014,** *88*, (3), 1046-55.
45. Han, X.; Shen, S.; Fan, Q.; Chen, G.; Archibong, E.; Dotti, G.; Liu, Z.; Gu, Z.; Wang, C. Red blood cell-derived nanoerythrosome for antigen delivery with enhanced cancer immunotherapy. *Science advances* **2019,** *5*, (10), eaaw6870.
46. Lejeune, A.; Moorjani, M.; Gicquaud, C.; Lacroix, J.; Poyet, P.; Gaudreault, R. Nanoerythrosome, a new derivative of erythrocyte ghost: preparation and antineoplastic potential as drug carrier for daunorubicin. *Anticancer research* **1994,** *14*, (3A), 915-9.
47. Janiak, J.; Bayati, S.; Galantini, L.; Pavel, N. V.; Schillen, K. Nanoparticles with a bicontinuous cubic internal structure formed by cationic and non-ionic surfactants and an anionic polyelectrolyte. *Langmuir* **2012,** *28*, (48), 16536-46.
48. Bhomia, R.; Trivedi, V.; Coleman, N. J.; Mitchell, J. C. The thermal and storage stability of bovine haemoglobin by ultraviolet-visible and circular dichroism spectroscopies. *Journal of pharmaceutical analysis* **2016,** *6*, (4), 242-248.
49. Konstantinova, I.; Lammert, E. Microvascular development: learning from pancreatic islets. *BioEssays* **2004,** *26*, (10), 1069-75.
50. Efrat, S.; Tal, M.; Lodish, H. F. The pancreatic beta-cell glucose sensor. *Trends in biochemical sciences* **1994,** *19*, (12), 535-8.
51. Ishihara, H.; Asano, T.; Tsukuda, K.; Katagiri, H.; Inukai, K.; Anai, M.; Kikuchi, M.; Yazaki, Y.; Miyazaki, J.; Oka, Y. Overexpression of hexokinase I but not GLUT1 glucose transporter alters concentration dependence of glucose-stimulated insulin secretion in pancreatic beta-cell line MIN6. *The Journal of biological chemistry* **1994,** *269*, (4), 3081-7.
52. Voigt, J.; Christensen, J.; Shastri, V. P. Differential uptake of nanoparticles by endothelial cells through polyelectrolytes with affinity for caveolae. *PNAS* **2014,** *111*, (8), 2942-7.

53. Tahir, S. A.; Ren, C.; Timme, T. L.; Gdor, Y.; Hoogeveen, R.; Morrisett, J. D.; Frolov, A.; Ayala, G.; Wheeler, T. M.; Thompson, T. C. Development of an immunoassay for serum caveolin-1: a novel biomarker for prostate cancer. *Clinical cancer research* **2003,** *9*, (10 Pt 1), 3653-9.
54. Xia, F.; Gao, X.; Kwan, E.; Lam, P. P.; Chan, L.; Sy, K.; Sheu, L.; Wheeler, M. B.; Gaisano, H. Y.; Tsushima, R. G. Disruption of pancreatic beta-cell lipid rafts modifies Kv2.1 channel gating and insulin exocytosis. *The Journal of biological chemistry* **2004,** *279*, (23), 24685-91.
55. Bahmani, B.; Bacon, D.; Anvari, B. Erythrocyte-derived photo-theranostic agents: hybrid nano-vesicles containing indocyanine green for near infrared imaging and therapeutic applications. *Scientific reports* **2013,** *3*, 2180.
56. Flower, R.; Peiretti, E.; Magnani, M.; Rossi, L.; Serafini, S.; Gryczynski, Z.; Gryczynski, I. Observation of erythrocyte dynamics in the retinal capillaries and choriocapillaris using ICG-loaded erythrocyte ghost cells. *Investigative ophthalmology & visual science* **2008,** *49*, (12), 5510-6.
57. Hu, C. M.; Zhang, L.; Aryal, S.; Cheung, C.; Fang, R. H.; Zhang, L. Erythrocyte membrane-camouflaged polymeric nanoparticles as a biomimetic delivery platform. *PNAS* **2011,** *108*, (27), 10980-5.
58. Fusco, J.; Xiao, X.; Prasadan, K.; Sheng, Q.; Chen, C.; Ming, Y. C.; Gittes, G. GLP-1/Exendin-4 induces beta-cell proliferation via the epidermal growth factor receptor. *Scientific reports* **2017,** *7*, (1), 9100.
59. Wang, P.; Yoo, B.; Yang, J.; Zhang, X.; Ross, A.; Pantazopoulos, P.; Dai, G.; Moore, A. GLP-1R-targeting magnetic nanoparticles for pancreatic islet imaging. *Diabetes* **2014,** *63*, (5), 1465-74.
60. Oram, R. A.; Sims, E. K.; Evans-Molina, C. Beta cells in type 1 diabetes: mass and function; sleeping or dead? *Diabetologia* **2019,** *62*, (4), 567-577.

TOC Graphic

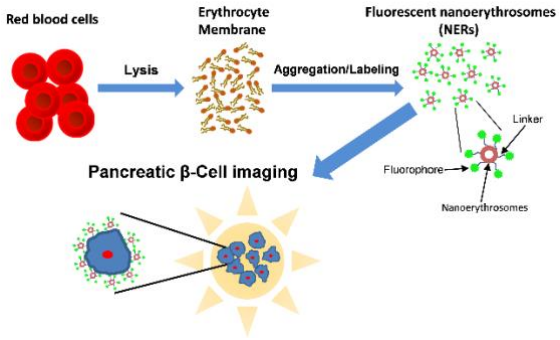
Red blood cells
Erythrocyte Membrane
Lysis
Aggregation/Labeling
Fluorescent nanoerythrosomes (NERs)
Linker
Fluorophore
Nanoerythrosomes
Pancreatic β-Cell imaging